Particle Accelerators, 1972, Vol. 3, pp. 235–244

FIELD DISTRIBUTION, POWER LOSSES AND PARAMETER OPTIMIZATION OF HELICAL ACCELERATOR STRUCTURES†

H. KLEIN, N. MERZ AND O. SIART‡

Institut für angewandte Physik der Universität Frankfurt/M., Germany

A method for the parameter optimization of a helix accelerator providing minimum total power losses is given. Approximate calculations of surface charge and current distribution on helical waveguides and their application to the problem of power losses and maximum field strengths are reported. Perturbation measurements of axial and surface fields in helix resonators were made and compared with theoretical results.

INTRODUCTION

First the parameter optimization of the helix accelerator (HELAC)[1] with respect to the dissipated rf power will be discussed, based on the sheath theory of the helix, especially on the expression of the shunt impedance given by Johnsen.[2] The latter uses a simple approximation in relating the sheath helix to the real round wire helix. To take into account the situation on the helix wire more precisely, computations were made, which will be reported in the following.

While minimization of power losses is desirable for normal conducting accelerators, reduction of maximum field strengths is of great importance for superconducting structures. Calculations and model measurements connected with this problem will be described.

1. PARAMETER OPTIMIZATION OF THE HELIX ACCELERATOR WITH RESPECT TO POWER LOSSES

Particles of charge e and mass m_0 are to be accelerated from the energy T_1 to the energy T_2. The quantity μ will be used as a measure of the particle velocity v

$$\mu = \beta/(1-\beta^2)^{1/2}, \quad \beta = v/c,$$
$$T = m_0c^2 \cdot ((1+\mu^2)^{1/2}-1).$$

To get the most effective acceleration from the rf power

$$P = \int_0^L p(z)\mathrm{d}z$$

(p losses per length, L accelerator length, z axial coordinate), one wishes to have a shunt impedance $\eta = E_0^2/p$ as large as possible (E_0 amplitude of the accelerating electric field on the axis).

In Ref. 3 it is shown for linear accelerators in general that the total power is proportional to the integral

$$A = \int_{T_1}^{T_2} \mathrm{d}T(\eta(T))^{-1/2}.$$

Hence one has to choose helix parameters and frequency in such a way that A becomes a minimum. This will be done in two steps.

Since the frequency must be constant along the accelerator at least for sections (frequency jumps are only possible in integer ratios), the helix parameters providing maximum shunt impedance are first evaluated along the accelerator for several constant frequencies. Then one has to calculate the integrals A and find the frequency or the set of frequencies yielding the smallest A-value.

The sheath theory of the helix gives the shunt impedance η as a function of the parameters x and b/a (see Fig. 5), with a factor containing directly the frequency f, the helix radius a, the pitch s or the phase velocity v_{ph} of the rf wave. Assuming the particle velocity v and v_{ph} to be equal, one has

$$x = \frac{2\pi}{c}\cdot\frac{a\cdot f}{\mu} = \frac{2\pi a}{\lambda}\cdot(1-\beta^2)^{1/2} \approx \frac{2\pi a}{\lambda}. \qquad (1)$$

λ is the axial wavelength. The dispersion relation yields

$$\mu = \frac{s}{2\pi a}\cdot\varepsilon(x,b/a), \qquad (2)$$

† Work supported by Bundesministerium für Bildung und Wissenschaft and GSI, Darmstadt.

‡ Staff member of GSI, Darmstadt.

where the function ε is given by

$$\varepsilon = [I_0 K_0 D_0/(I_1 K_1 D_1)]^{1/2}$$

with $D_0 = 1 - I_0\bar{K}_0/(K_0\bar{I}_0)$, $D_1 = 1 - I_1\bar{K}_1/(K_1\bar{I}_1)$, and I_0, K_0, I_1, K_1 are modified Bessel functions of the arguments x and $x \cdot b/a$, the latter indicated by the bar.

The following expressions of η will be used[2,4,5]:

$$\begin{aligned}\eta &= \mu^{-1} \cdot f^{1/2} \cdot [C \cdot x \cdot \eta_0(x,b/a)] \\ &= \mu^{-1} \cdot f^{1/2} \cdot \eta_\mu \\ &= s^{-1/2} \cdot [C \cdot c^{1/2} \cdot x^{3/2} \cdot \eta_0(x,b/a) \cdot (\varepsilon(x,b/a))^{-1/2}] \\ &= s^{-1/2} \cdot \eta_s \\ &= a^{-1} \cdot f^{-1/2} \cdot [C \cdot c/2\pi \cdot x^2 \cdot \eta_0(x,b/a)] \\ &= a^{-1} \cdot f^{-1/2} \cdot \eta_a. \end{aligned} \qquad (3)$$

For normal conducting helices (conductivity κ) and travelling waves is

$$C = 0.476 \cdot \kappa^{1/2}\ [M\Omega/m \cdot \mathrm{MHz}^{-1/2}],\ \kappa \text{ in } m/\Omega\mathrm{mm}^2.$$

A frequency-dependent improvement factor is necessary in case of superconductivity.

With some approximations[4] the function η_0 can be written as

$$\eta_0 = \frac{(K_0/I_0) \cdot D_0 \cdot (K_1/I_1) \cdot D_1}{(I_1^2 \cdot \pi/4)^{-1} + (I_1^2 \cdot b/a)^{-1}}. \qquad (4)$$

For reasons of simplicity the ratio b/a is assumed to be large ($\gtrsim 5$) and constant (negligible influence of the outer conductor). η_μ, η_s, η_a as functions of x describe the shunt impedance for constant particle energy, constant helix pitch, constant helix radius. They have maxima at

$$x_\mu \approx 0.4, \quad x_s \approx 0.7, \quad x_a \approx 0.9.$$

The η-curves for μ_1 and μ_2 (Fig. 1) correspond to the initial and the final energy T_1, T_2 in the accelerator.

To get highest possible η-values during acceleration one should keep constant $x = x_\mu$ and so be always at the maximum of the η_μ-curve ($1^* \to 2$ in Fig. 1). But in a HELAC there are minimum values of winding diameter and distance $s_{\min}$ and and helix radius $a_{\min}$ which are fixed by consideration of coolant flux and beam diameter. Therefore attainable η-values are limited by the curves belonging to $s = s_{\min}$ and $a = a_{\min}$. Consequently the transition from μ_1 to μ_2 is led along these curves until $x = x_\mu$ is reached ($1 \to 2$ in Fig. 1).

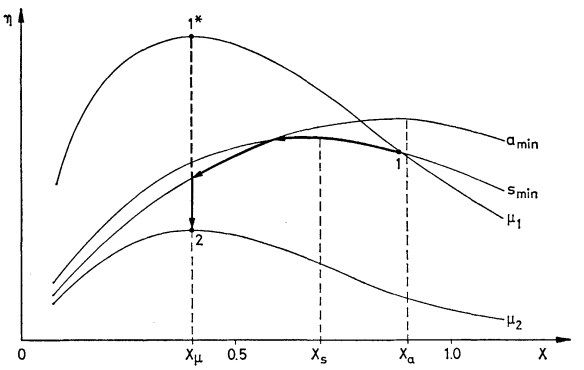

FIG. 1. Sketch of shunt impedance η versus helix parameter x for constant μ (particle velocity), s (helix pitch) and a (helix radius) at constant frequency and negligible influence of outer conductor.
$1 \to 2$: maximal η for acceleration from μ_1 to μ_2, restricted by minimal pitch $s_{\min}$ and radius $a_{\min}$.
$1^* \to 2$: maximal η without restriction.
x_μ, x_s, x_a: x-values of the maxima of the η-curves.

Since the continuous variation of helix radius a would not be useful, the curve branches $s = s_{\min}$ and $x = x_\mu$ will be approximated actually by stepwise constant a. In this way the helix parameters providing maximum shunt impedance $\eta_{\max}$ at constant frequencies are determined.

In the second step the optimal frequency is found. As an example in Fig. 2 the function $(\eta_{\max}(T))^{-1/2}$ is plotted for proton acceleration from $T_1 = 1$ MeV to $T_2 = 20$ MeV at several

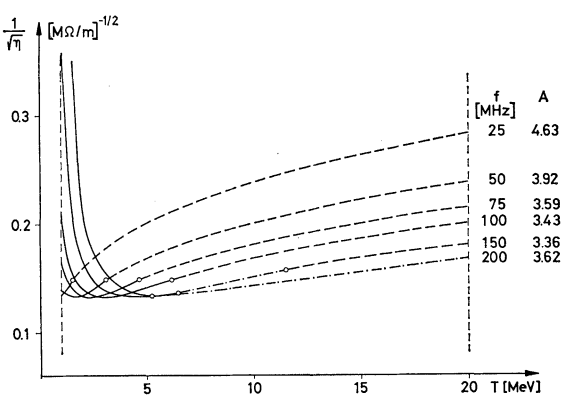

FIG. 2. $\eta^{-1/2}$ versus particle energy T at various frequencies f for proton acceleration from 1 MeV to 20 MeV ($b/a = 5$).
———: $s = s_{\min} = 1$ cm;
—·—·: $a = a_{\min} = 2$ cm;
— — —: $x = x_\mu = 0.4$
$A = \int dT\, \eta^{-1/2}$ optimization area (arbitrary units).

frequencies and the values of the integral $A = \int dT(\eta_{max})^{-1/2}$ are given ($s_{min} = 1$ cm, $a_{min} = 2$ cm). The optimal frequency is 150 MHz, belonging to the smallest A-value. For this frequency the helix parameters along the accelerator are plotted in Fig. 3. It is noticeable that the helix radius decreases at first, whereas it increases at higher energies.

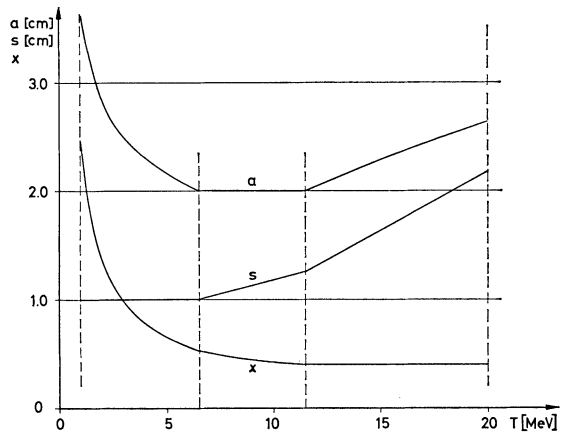

FIG. 3. Helix parameter x, pitch s, radius a providing maximum shunt impedance along a proton accelerator at the frequency $f = 150$ MHz.

This optimization method has to be modified slightly, if instead of the condition $b/a = \text{const}$ a constant radius b of the outer conductor is given. In this case a increases to a smaller degree, since increasing a would cause additional losses on the outer conductor and therefore lead to disadvantageous η-values.

2. APPROXIMATE CALCULATION OF POWER LOSSES ON ROUND WIRE HELICES

Johnsen's shunt impedance formula (3), (4) is fairly well suited for real wire helices as measurements show. In general, measured losses are somewhat greater than the theoretical values, increasing with frequency or parameter x, whereas at small x-values smaller losses may occur.

In order to evaluate helix losses more precisely and to investigate their parameter dependence, a method for the approximate calculation of surface current distributions on round wire helices was developed.[6] For this purpose, the helix windings are replaced by a series of circular rings with distances equal to the helix pitch s, carrying a sinusoidal total current distribution, the axial wavelength λ of which is taken from the sheath theory.

On this ring model of the helix, the surface current density i is calculated in quasi-stationary approximation (see Appendix). The integral equation of the current distribution is transformed in a linear equation system and numerically solved. Using imaging planes and integer values of $\lambda/2s$, one may restrict the calculation to a $\lambda/4$-part of the whole structure, which is assumed to be infinitely extended (i.e., end effects are neglected). To calculate the losses, one must integrate i^2 over the conductor surface and multiply by the surface resistance. This value is proportional to the square of the total current amplitude I. To give the shunt impedance one must know the electric axial field strength E_0 belonging to I. One might suppose that the ratio I/E_0 for round wire helices could be taken from the sheath theory, as Johnsen did, deriving his shunt impedance formula. However, ring model calculations of electric fields as well as measurements indicate that for a given axial electric field the total charge and current amplitudes on round wire helices exceed those on similar sheath helices. Apparently this difference is caused by the field concentration in the proximity of the windings, which increases with the ratio d/s (d = wire diameter) as will be shown in the following paragraph.

A result relevant to parameter optimization is that helix losses become minimal for d/s in the range 0.5–0.7.

Figure 4 shows losses, calculated with the ring model and related to results from Johnsen's formula together with experimental values, plotted against the parameter x. The values are similar except for a difference of about 10%. A main reason for this difference is thought to be additional losses caused by surface roughness which were not taken into account.

As the figures show, results yielded by another calculational method for surface fields (CT), which will be described in the next paragraph, do not differ much from ring model values of power losses.

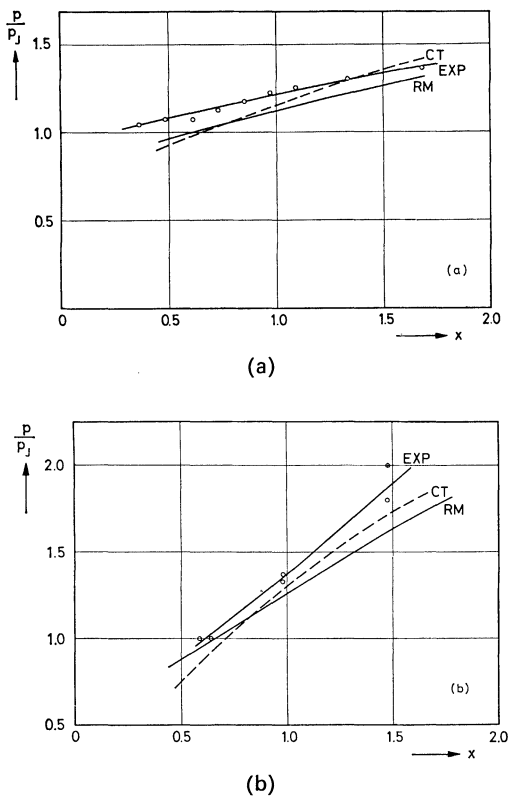

FIG. 4. Helix losses p in relation to Johnsen's approximation p_J, EXP experimental values, RM ring model values, CT calculated according to Ref. 9.
Parameters: (*a*) $d/s = 0.56$, $\tan\psi = 0.052$, $b/a = 5.6$
(*b*) $d/s = 0.66$, $\tan\psi = 0.016$, $b/a = 2.0$

3. CALCULATION OF MAXIMUM FIELD STRENGTHS

For superconducting helix accelerators the maximum magnetic field strength H^{max} and, as measurements show,[7,8] the maximum electric field strength E^{max} as well are critical quantities. Therefore, knowledge of the relations between maximum field strengths and the accelerating axial field is essential for the design of accelerators.

The distribution of surface currents or the tangential magnetic field on helices carrying rf waves has been calculated approximately by use of the ring model. Thus, information on maximum magnetic fields is given. A similar calculation concerning the distribution of surface charges or the normal electric field is easily made (see Appendix). It turns out that with the total current and charge varying sinusoidally along the series of rings, corresponding quantities such as magnetic flux, voltage, field strengths on the axis, etc. vary likewise sinusoidally to a good approximation. It is useful to relate all quantities to the electric field amplitude on the axis E_{ax} (a standing wave of amplitude E_{ax} on the axis of a helix resonator has an accelerating component $E_0 = E_{ax}/2$). From a ring model calculation with arbitrary charge amplitude q the ratios E^{max}/q, E_{ax}/q and hence E^{max}/E_{ax} are available.

A magnetic field computation in a ring model with a current amplitude I yields H^{max}/I first. One gets H^{max}/E_{ax} applying E_{ax}/q and an appropriate value of I/q. That means, I must be related to q in a way which is valid for wave propagation on helices. Since I/q represents the phase velocity of the wave (see Appendix), which is determined by the sheath theory in good accordance with measurements, this relation can be taken from the sheath theory.

The results of these calculations depend only on ratios of lengths. The following parameters have been chosen:

$$d/s,\ s/2\pi a = \tan\psi,\ \lambda/2s = N,\ b/a.$$

The helix parameter x can be written in the form

$$x \approx (2 \cdot N \cdot \tan\psi)^{-1}.$$

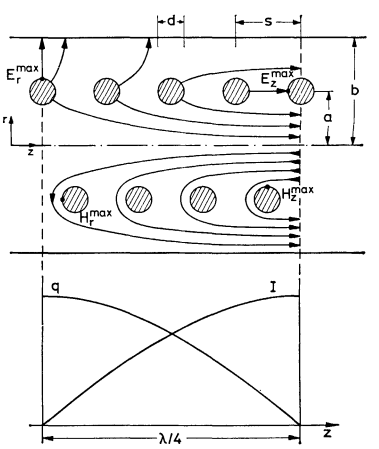

FIG. 5. Field configuration and distribution of total charge q and current I in a $\lambda/4$ part of a standing helix wave.

As indicated in Fig. 5 there are the following

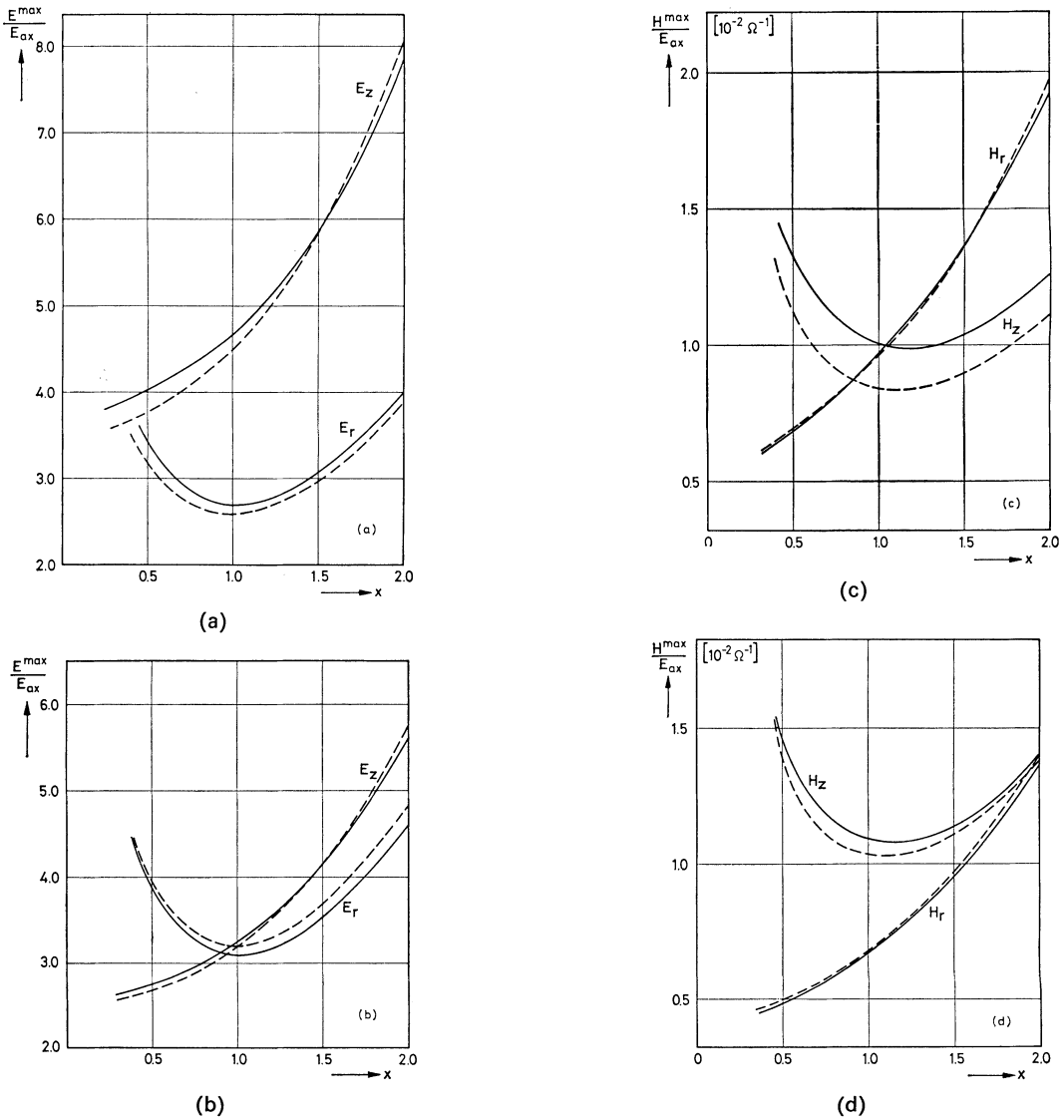

FIG. 6 Maximal field strengths E^{max}, H^{max} in terms of the axial electric field E_{ax} versus x. ———: ring model results for $\tan\psi = 0.04$, $b/a = 3$; – – –: CT values (Ref. 9) for $b/a = 3$; (*a*) electric field, $d/s = 0.7$; (*b*) electric field, $d/s = 0.5$; (*c*) magnetic field, $d/s = 0.7$; (*d*) magnetic field, $d/s = 0.5$.

maxima of field strength in the case of standing waves:

E_r^{max} on the outer side of the winding in the antinode of total charge,

E_z^{max} on the winding parts next to adjacent windings in the node of total charge,

H_z^{max} on the inner side of the winding in the antinode of total current,

H_r^{max} on the winding parts next to adjacent windings in the node of total current.

In Fig. 6 ring model results for some parameters are plotted against x. Main features are:

1. With x, E_z^{max}, H_r^{max} increase, whereas E_r^{max}, H_z^{max} pass through minima.
2. With d/s, E_z^{max}, H_r^{max} increase, whereas E_r^{max}, H_z^{max} decrease.
3. With b/a, all values decrease asymptotically, at small x in a greater degree than at large x.
4. The dependence on N or $\tan\psi$ at constant x is small.

Another method to calculate the electromagnetic field strengths around helices is described in Ref. 9 (CT). Substituting parallel cylinders for the helix windings, the field distribution is determined by conformal mapping. The field strengths at large distance from this cylinder grating are assumed to converge to values which are given by the sheath theory as field amplitudes on the surface of the helical sheath:

$$E_z = |E_z(r=a)| \qquad E_r^{0,i} = |E_r(r=a\pm 0)|$$
$$H_r = |H_r(r=a)| \qquad H_z^{0,i} = |H_z(r=a\pm 0)|. \tag{5}$$

These quantities in terms of the electric field strength on the axis, are functions of x and b/a.

Cylinder grating calculations result in field enhancement factors, X, Y, depending only on d/s, which must multiply the sheath theory values to give the maximum field strengths:

$$E_z^{\max} = X \cdot E_z \qquad E_r^{\max} = Y \cdot E_r^{0}$$
$$H_r^{\max} = X \cdot H_r \qquad H_z^{\max} = Y \cdot H_z^{i}. \tag{6}$$

Values obtained from this method are included in Fig. 6. These show that differences to ring model values are not large.

To facilitate comparisons and applications ring model values can be expressed approximately in the form of formula (6). Averaging over $\tan\psi$, N, b/a one gets enhancement factors (X_E, Y_E, X_H, Y_H) slightly different for electric and magnetic fields. From ring model calculations in the parameter range

$$0.3 \leqq d/s \leqq 0.7, \quad 0.02 \leqq \tan\psi \leqq 0.1,$$
$$6 \leqq N \leqq 24, \quad b/a \geqq 2$$

result enhancement factors as shown in Fig. 7. (Curve X_2 in Fig. 7a represents the field enhancement calculated for two parallel cylinders.[4]) Maximum field strengths calculated with these factors deviate from the exact ring model values by at most 7%.

The ratios of maximum and axial fields show the following minima (for $b/a \to \infty$):

$$\frac{E^{\max}}{E_{ax}} = 2.95 \quad \text{at} \quad d/s = 0.52 \quad \text{and} \quad x = 0.7,$$
$$\frac{H^{\max}}{E_{ax}} = 0.98 \cdot 10^{-2}\Omega^{-1}\left(123\,\frac{\text{G}}{\text{MV/m}}\right)$$
$$\text{at} \quad d/s = 0.68 \quad \text{and} \quad x = 1.1.$$

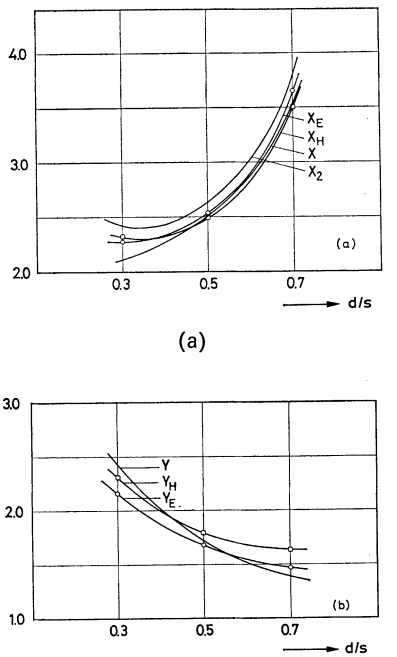

(a)

(b)

FIG. 7. Field enhancement factors to be applied to sheath helix values, plotted against the ratio d/s.
(*a*) X_E (valid for E_z), X_H (valid for H_r) ring model approximation, X values from Ref. 9, X_2 two cylinder approximation (Ref. 4).
(*b*) Y_E (valid for E_r), Y_H (valid for H_z) ring model approximation, Y values from Ref. 9.

A similar approximate expression can be found for the factor which multiplies the sheath helix current amplitude I_{sh} to give the wire helix current I in case of equal axial electric field. It is

$$\frac{I}{I_{\text{sh}}} \approx 1 + \frac{\alpha(d/s)}{N} \tag{7}$$

with a function α given in Fig. 8. (The ring model value of $H^{\max}$, quoted in Ref. 7, is calculated

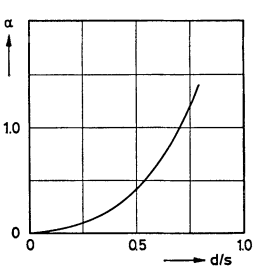

FIG. 8. The function $\alpha(d/s)$.

assuming $I = I_{sh}$. The correction gives a value higher by 25%.)

4. FIELD MEASUREMENTS

Perturbation measurements in helix resonators were made to investigate axial field strengths in relation to the dissipated rf power, as well as maximum field strengths.[10,11] Two principal objectives were pursued: First, agreement with calculations should be checked. As the theory is valid for long helices, resonators extending over some wavelengths (up to 15 $\lambda/2$) were measured.

Secondly, in connection with the Karlsruhe measurements with superconducting helix resonators,[7,8] the attainable maximum field strengths had to be determined, corresponding to the breakdown values of power and Q. As these measurements were made with short $\lambda/2$ helices, for which calculations are difficult (a theory of end effects is in preparation), the experimental method was the only practicable one.

The perturbation method becomes erroneous in the vicinity of conducting surfaces, thus presenting a difficulty, since the interesting peak fields occur on the conductor surfaces. However experimental results turn out to be in good agreement with the theoretical values. This means for example, that a perturbation object located in the middle of the gap between two windings of a long helix yields a field value, which lies reasonably between the maximum and the minimum value, calculated for this region. Concluding that theoretical field strengths for a long helix are correct, one may use the ratio of the theoretical maximum and the measured value to multiply the measured value for a short helix of equal dimensions and resonance frequency. The experimental error is considered to be the same in either case. Maximum field strengths in $\lambda/2$ helices were determined in this way.

Helices wound of copper tube were mounted in the outer conductor by means of a removable cage of copper bars and rings. The hinged top part of the outer cylinder rendered accessible the helix under investigation. End plates were located at a distance of about 15 cm from the helix ends. The ends formed short-circuit connections with the outer conductor. Small teflon and bronze beads attached to nylon threads could be moved longitudinally and radially through the resonator by use of a pulley system. As a measure for the resonator frequency shift, Δf, produced by these perturbation objects, the phase shift, $\Delta\varphi$, was recorded as a function of the location of the objects by a plotter. Calibration was performed by changing the generator frequency.

This phase method is advantageous for low Q resonators. With Q values of 2000 and relative frequency shifts of 3×10^{-6}, the sensitivity of the phase shift exceeds that of the amplitude resonance by a factor of 100.

The relative frequency shift $\Delta f/f$ caused by dielectric and metallic perturbation objects can be written in the form[12]

$$\begin{aligned} \Delta f_D/f &= -g_D \cdot 2\pi f \cdot \varepsilon_0 \cdot E^2/(P \cdot Q) \\ \Delta f_M/f &= -g_M \cdot 2\pi f \cdot (\varepsilon_0 E^2 - \tfrac{1}{2}\mu_0 H^2)/(P \cdot Q) \end{aligned} \tag{8}$$

where E, H are the field strengths at the point of the perturbation object, Q, P are Q-value (unloaded) and power losses of the resonator, g_D, g_M are perturbation constants.

Dielectric spheres of radius r_D and relative permittivity ε and metallic spheres of radius r_M have perturbation constants

$$g_D = \pi {r_D}^3 \frac{\varepsilon - 1}{\varepsilon + 2} \qquad g_M = \pi {r_M}^3. \tag{9}$$

These constants were checked by control measurements in a rectangular cavity resonator.

Perturbation measurements result in field strength values expressed in terms of resonator Q and power losses:

$$E' = E \cdot (P \cdot Q)^{-1/2} \qquad H' = H \cdot (P \cdot Q)^{-1/2}.$$

Therefore, the quantities E', H', obtained with model resonators at small generator powers of some milliwatts, may be applied to high power accelerator sections of the same shape, provided that the actual Q value and the transmitted power are known. Furthermore the phase method is appropriate for measuring of the shunt impedance η without additional Q determination. A dielectric perturbation object on the axis of an accelerator section causes a maximum frequency shift

$$\Delta f/f \propto {E_0}^2/(P \cdot Q) \propto \eta/Q.$$

TABLE I

Axial and maximum field strengths in helix resonators (Parameters in Table II)

	Long helix ($7\lambda/2$)					Short helix ($\lambda/2$)		
	Sheath theory	Measured	Ring model	Correction factor	$\frac{E^{max}}{E_{ax}}, \frac{H^{max}}{H_{ax}}$	Measured	Corrected	$\frac{E^{max}}{E_{ax}}, \frac{H^{max}}{H_{ax}}$
E'_{ax}	0.217	0.208→	0.208			0.346		
E'^{max}_z	0.263	0.65	0.79(0.61)†	1.21	3.80	1.25	1.51	4.37
E'^{max}_r	0.495	0.45	0.75	1.66	3.60	0.83	1.38	4.00
H'_{ax}	1.15	1.22				2.31		
H'^{max}_r	0.57	1.48	1.64(1.27)†	1.11	1.34	3.15	3.50	1.51
H'^{max}_z	1.39	1.60	2.34	1.46	1.92	3.55	5.19	2.25

$E' = E \cdot (PQ)^{1/2}[10^{-3}\ \mathrm{MV/m \cdot W^{-1/2}}]$, $H' = H \cdot (PQ)^{1/2}[\mathrm{A/m \cdot W^{-1/2}}]$

† Minimum value in the wire interspace

The corresponding phase shift is in very good approximation

$$\Delta\varphi = 2 \cdot Q \cdot \Delta f/f,$$

therefore is

$$\Delta\varphi \propto \eta.$$

Table I shows field strengths for a pair of helices, the parameters of which are given in Table II.

TABLE II

Helix parameters

	Long helix ($7\lambda/2$)	Short helix ($\lambda/2$)
Outer conductor radius b	6.5 cm	
Helix radius a	3.22 cm	
Helix pitch s	0.98 cm	
Wire diameter d	0.61 cm	
Node distance $\lambda/2$	11.05 cm	12.8 cm
Resonance frequency f	79.1 MHz	78.9 MHz
Number of windings per $\lambda/2$	11.5	13
Q-value	1805	1720
x-value	0.9	—

Ring model results for the long helix are based on the measured electric field amplitude on the axis. Due to field concentration around the helix wire, this value is smaller than the sheath theory value, the reference quantity is the stored electromagnetic energy which is proportional to $P \cdot Q$. On the other hand, the measured magnetic field amplitude on the axis H_{ax} exceeds the sheath helix value, thus indicating a higher current in wire helices as mentioned above. This behaviour is exemplified as well by Fig. 9 which shows measured and theoretical axial field strengths over a range of x.

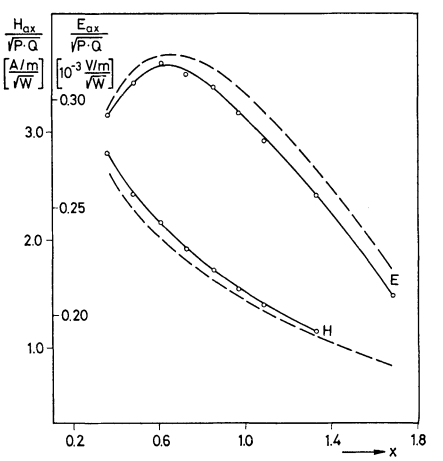

FIG. 9. Field strength amplitudes on the axis of a helix resonator versus x.
———: perturbation measurements;
— — —: sheath theory values
Parameters: $a = 2.23$ cm, $s = 0.72$ cm, $d = 0.4$ cm, $b = 12.5$ cm.

To measure the peak fields, spheres of 3 mm diameter were moved longitudinally at a surface distance of about 0.5 mm along the helices and radially in the winding interspaces. Examples of plotter graphs for the $\lambda/2$ helix are given in Fig. 10. In Table I the application of correction factors, derived from long helix values to short helix measurements, is evident. Short helices show a more disadvantageous relation between axial and

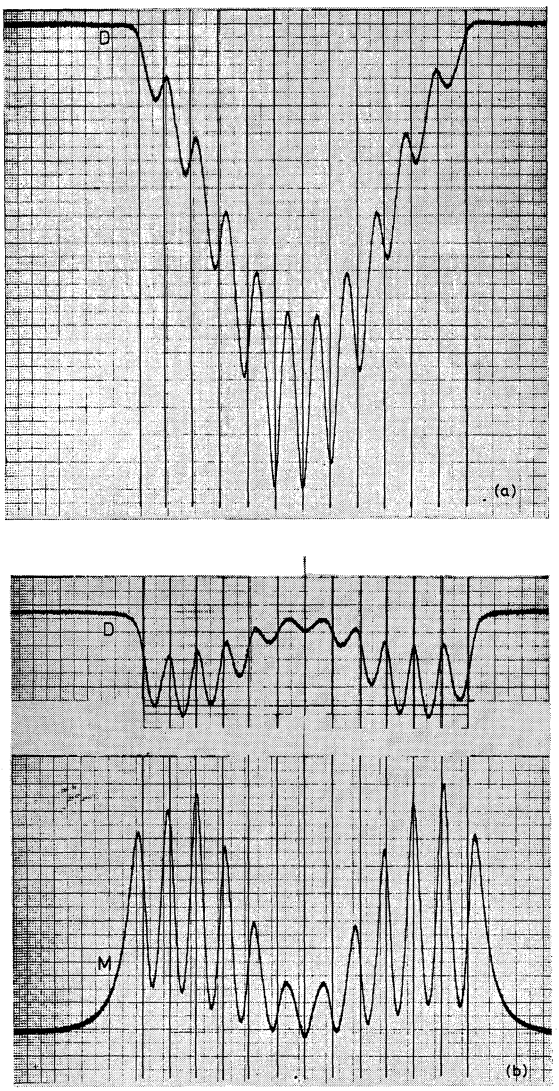

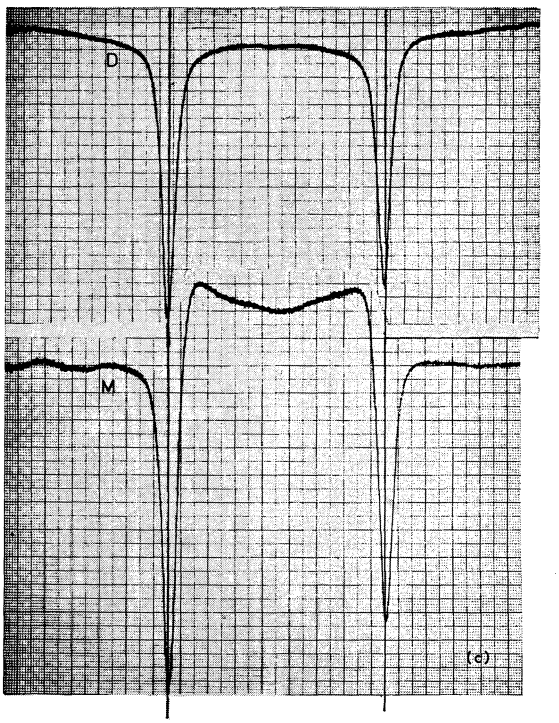

FIG. 10. Plotter graphs of perturbation measurements near the winding surface of a $\lambda/2$-helix (dimensions in Table II), D with dielectric bead, M with metallic bead. Winding positions marked by straight lines. (*a*) longitudinal at the outer side; (*b*) longitudinal at the inner side; (*c*) radial between two end windings.

maximal fields than long ones. In Table I the enhancement of short helix peak values is higher by 10–15%.

APPENDIX

Integral Equations of Charge and Current Distribution on the Ring Model

A very long, perfectly conducting helix carrying an electromagnetic wave of frequency f and axial wave length λ is assumed. The relation between surface charge σ, surface current i, normal and tangential components of surface fields are

$$E_n = \sigma, \qquad H_t = i, \tag{A.1}$$

$$E_t = 0, \qquad H_n = 0. \tag{A.2}$$

Assuming $\lambda \ll \lambda_0 = c/f$ and omitting retardation the static form of the electromagnetic potentials may be used.

If the wavelength λ is much greater than the helix pitch s, variations along one winding are negligible. Thus each winding can be replaced by a circular ring, having net charge and current, the values of which vary sinusoidally from ring to ring. Further-

more rotational symmetry occurs. The electromagnetic potentials are given by

$$V(\mathbf{x}) = \frac{1}{2\pi r} \cdot \int \mathrm{d}s' \cdot \sigma(\mathbf{x}') \cdot K_E(\mathbf{x},\mathbf{x}'), \quad \text{(A.3)}$$

$$A(\mathbf{x}) = \frac{1}{2\pi r} \cdot \int \mathrm{d}s' \cdot i(\mathbf{x}') \cdot K_H(\mathbf{x},\mathbf{x}'), \quad \text{(A.4)}$$

where

$\mathbf{x} = (r,z)$ is an arbitrary point in the longitudinal section of the structure,
$\mathbf{x}' = (r',z')$ is a point on a conducting surface,
$\mathrm{d}s'$ is the line element on a conducting surface in the (r,z)-plane,
V is the electric potential,
A is the azimuthal component of the magnetic vector potential,
$K_E = (rr')^{1/2} \cdot k \cdot K(k)$,
$K_H = (rr')^{1/2} \cdot [(2/k-k) \cdot K(k) - 2/k \cdot E(k)]$,
$K(k)$, $E(k)$ are complete elliptic integrals of the modulus k,
$k = (4rr'/[(z-z')^2+(r+r')^2])^{1/2}$.

From (A.2) it follows that the potential V and the magnetic flux function $\phi = 2\pi r \cdot A$ must be constant on conductor surfaces (on the outer conductor the constant is zero). For surface points $\mathbf{x} = (r,z)$ on conductors labeled by n, one has the relations

$$\frac{1}{2\pi r} \cdot \sum_{n'} \int_{n'} \mathrm{d}s' \sigma(\mathbf{x}') \cdot K_E(\mathbf{x},\mathbf{x}') = V_n(\mathbf{x}) = V_n, \quad \text{(A.5)}$$

$$\sum_{n'} \int_{n'} \mathrm{d}s' i(\mathbf{x}') \cdot K_H(\mathbf{x},\mathbf{x}') = \phi_n(\mathbf{x}) = \phi_n, \quad \text{(A.6)}$$

together with

$$\int_n \mathrm{d}s \cdot 2\pi r \cdot \sigma(\mathbf{x}) = q_n = q \cdot \cos 2\pi z_n/\lambda, \quad \text{(A.7)}$$

$$\int_n \mathrm{d}s \cdot i(\mathbf{x}) = I_n = I \cdot \sin 2\pi z_n/\lambda, \quad \text{(A.8)}$$

$$(z_{n+1} - z_n = s),$$

I_n, q_n being net charge and current of the rings.

These are integral equations for the surface charge and current distribution, which must be solved numerically.

The relation for q and I is taken from the sheath theory. On the sheath helix the current amplitude is defined by

$$I = s \cdot (H_z^{\,i} + H_z^{\,0}) \quad \text{[see Eq. (5)]} \quad \text{(A.9)}$$

and the amplitude of charge per axial length by

$$q' = q/s = 2\pi a \cdot (E_r^{\,i} + E_r^{\,0}) \quad \text{[see Eq. (5)].} \quad \text{(A.10)}$$

The ratio is

$$\frac{I}{q'} = \frac{v_{\mathrm{ph}}}{c} \cdot \frac{1}{Z_0} \approx \frac{s}{2\pi a} \cdot \varepsilon(x,b/a) \cdot \frac{1}{Z_0} \text{ [see Eq. (2)]} \quad \text{(A.11)}$$

$$(Z_0 = 120\ \pi\Omega).$$

REFERENCES

1. H. Klein, P. Junior, J. Klabunde, O. Siart, H. Deitinghoff, P. Finke, and A. Schempp, *Proc. Intern. Conf. Nucl. React. Induced by Heavy Ions, Heidelberg 1969*, p. 540.
2. K. Johnsen, Chr. Michelsen Inst. Beretn. 16, Bergen (1954). Report CERN-PS/KS 27 (1954).
3. H. Klein and O. Siart, *1970 Proc. Prot. Lin. Acc. Conf., NAL, Batavia*, p. 293.
4. H. Klein, Habilitationsschrift Univ. Frankfurt/M. (1968).
5. H. Schopper, Kernforschungszentrum Karlsruhe, Bericht Nr. 1029 (1969).
6. O. Siart, Dissertation Univ. Frankfurt/M. (1970).
7. J. Fricke, H. Klein, B. Piosczyk, and J. E. Vetter, *Particle Accelerators*, **3**, 35 (1972).
8. A. Citron, J. L. Fricke, C. M. Jones, H. Klein, M. Kuntze, B. Piosczyk, D. Schulze, H. Strube, J. E. Vetter, N. Merz, A. Schempp, and O. Siart, *VIIIth Intern. Conf. on High Energy Accelerators, Geneva 1971*, p. 278.
9. A. J. Sierk, C. J. Hamer, and T. A. Tombrello, *Particle Accelerators*, **2**, 149 (1971).
10. N. Merz, Diplomarbeit Univ. Frankfurt/M. (1972).
11. P. Finkle, Diplomarbeit Univ. Frankfurt/M. (1970).
12. L. B. Mullett, Report AERE G/R 853, Harwell (1952).

Received 13 April 1972